

Northumbria Research Link

Citation: Vo, Thuc and Lee, Jaehong (2009) On sixfold coupled buckling of thin-walled composite beams. *Composite Structures*, 90 (3). 295 - 303. ISSN 0263-8223

Published by: Elsevier

URL: <http://dx.doi.org/10.1016/j.compstruct.2009.03.008>
<<http://dx.doi.org/10.1016/j.compstruct.2009.03.008>>

This version was downloaded from Northumbria Research Link:
<http://nrl.northumbria.ac.uk/13368/>

Northumbria University has developed Northumbria Research Link (NRL) to enable users to access the University's research output. Copyright © and moral rights for items on NRL are retained by the individual author(s) and/or other copyright owners. Single copies of full items can be reproduced, displayed or performed, and given to third parties in any format or medium for personal research or study, educational, or not-for-profit purposes without prior permission or charge, provided the authors, title and full bibliographic details are given, as well as a hyperlink and/or URL to the original metadata page. The content must not be changed in any way. Full items must not be sold commercially in any format or medium without formal permission of the copyright holder. The full policy is available online: <http://nrl.northumbria.ac.uk/policies.html>

This document may differ from the final, published version of the research and has been made available online in accordance with publisher policies. To read and/or cite from the published version of the research, please visit the publisher's website (a subscription may be required.)

www.northumbria.ac.uk/nrl



1 On sixfold coupled buckling of thin-walled composite beams

2 Thuc Phuong Vo* and Jaehong Lee†

3 *Department of Architectural Engineering, Sejong University*
4 *98 Kunja Dong, Kwangjin Ku, Seoul 143-747, Korea*

5 (Dated: March 12, 2009)

A general analytical model based on shear-deformable beam theory has been developed to study the flexural-torsional coupled buckling of thin-walled composite beams with arbitrary lay-ups under axial load. This model accounts for all the structural coupling coming from the material anisotropy. The seven governing differential equations for coupled flexural-torsional-shearing buckling are derived. The resulting coupling is referred to as sixfold coupled buckling. Numerical results are obtained for thin-walled composite beams to investigate effects of shear deformation, fiber orientation and modulus ratio on the critical buckling loads and corresponding mode shapes.

6 **Keywords:** Thin-walled composite beams; shear deformation; flexural-torsional-shearing buckling.

7 I. INTRODUCTION

8 Fiber-reinforced plastics (FRP) have been used over the past few decades in a variety of structures. Composites
9 have many desirable characteristics, such as high ratio of stiffness and strength to weight, corrosion resistance and
10 magnetic transparency. Thin-walled structural shapes made up of composite materials, which are usually produced by
11 pultrusion, are being increasingly used in many engineering fields. However, the structural behavior is very complex
12 due to coupling effects as well as warping-torsion and thus, the accurate prediction of stability limit state and dynamic
13 characteristics is of the fundamental importance in the design of thin-walled composite structures.

14 The theory of thin-walled open section members made of isotropic materials was first developed by Vlasov [1] and
15 Gjelsvik [2]. Up to the present, investigation into the stability behavior of these members has received widespread
16 attention and has been carried out extensively. Closed-form solution for flexural and torsional buckling of isotropic
17 thin-walled beams are found in the literature (Timoshenko [3], Trahair [4]). For thin-walled composite beams, the
18 flexural and torsional buckling are fully coupled even for a doubly symmetric cross-section due to their material
19 anisotropy. Based on a Vlasov-type linear hypothesis, Pandey et al. [5] investigated flexural-torsional stability of
20 thin-walled composite I-section beams. A finite element having seven degrees of freedom at each node was developed

*Graduate student

†Professor, corresponding author. Tel.:+82-2-3408-3287; fax:+82-2-3408-3331

; Electronic address: jhlee@sejong.ac.kr

21 by Lin et al. [6] to study the stability problem of thin-walled composite beams. The influence of the in plane shear
22 strain on the stability of the members was considered. Shield and Morey [7] developed a new theory for analysis
23 buckling of composite beams of open and closed cross section. The theory took into account deformation in the plane
24 of the cross section due to anticlastic curvature. Kollar [8-10] focused on the analysis of flexural-torsional buckling and
25 vibration of thin-walled open section composite beams. Vlasov's classical theory of thin-walled beams was modified to
26 include both the transverse shear and the restrained warping induced shear deformations. The works of Davalos, Qiao
27 and coworkers [11-13] deserved special attention because they presented a comprehensive experimental and analytical
28 approach to study flexural-torsional buckling behavior of full-size pultruded FRP I-beams and channel section. An
29 energy method based on nonlinear plate theory was developed for instability of FRP beams and the formulation
30 included shear effect and bending-twisting coupling. The monograph of Librescu and Song [14] was concerned not
31 only with the foundation and formulation of modern linear and nonlinear theories of thin-walled composite beams
32 but also provided powerful mathematical tools to address issues of statics and dynamics of these members. Cortinez,
33 Piovan, Machado and coworkers [15-18] introduced a new theoretical model for the generalized linear analysis of
34 thin-walled composite beams. This model allowed studying many problems of static's, free vibrations with or without
35 arbitrary initial stresses and linear stability of composite thin-walled beams. In their research [15-18], thin-walled
36 composite beams for both open and closed cross-sections and the shear flexibility (bending, non-uniform warping) were
37 incorporated. However, it was strictly valid for symmetric balanced laminates and especially orthotropic laminates.
38 Back and Will [19] developed a shear-flexible finite element based on an orthogonal Cartesian coordinate system for
39 the flexural and buckling analyses of thin-walled composite I-beams with both doubly and mono-symmetrical cross-
40 sections. Using the first-order shear deformable beam theory, the beam element included both the transverse shear
41 and restrained warping were derived. Recently, a simple but efficient method to evaluate the exact element stiffness
42 matrix was presented by Kim et al. [20,21] in order to perform the spatially coupled stability analysis of thin-walled
43 composite beams with symmetric and arbitrary laminations under a compressive force.

44 In this paper, which is an extension of the authors' previous works [22-25], flexural-torsional coupled buckling
45 of thin-walled composite beams with arbitrary lay-ups is presented. This model is based on the first-order shear-
46 deformable beam theory, and accounts for all the structural coupling coming from the material anisotropy. The seven
47 governing differential equations for coupled flexural-torsional-shearing buckling are derived. Numerical results are
48 obtained to investigate the effects of fiber angle, span-to-height ratio and modulus ratio on the critical buckling loads
49 and corresponding mode shapes of thin-walled composite beams.

50 II. KINEMATICS

51 The theoretical developments presented in this paper require two sets of coordinate systems which are mutually
 52 interrelated. The first coordinate system is the orthogonal Cartesian coordinate system (x, y, z) , for which the x and
 53 y axes lie in the plane of the cross section and the z axis parallel to the longitudinal axis of the beam. The second
 54 coordinate system is the local plate coordinate (n, s, z) as shown in Fig.1, wherein the n axis is normal to the middle
 55 surface of a plate element, the s axis is tangent to the middle surface and is directed along the contour line of the
 56 cross section. The (n, s, z) and (x, y, z) coordinate systems are related through an angle of orientation θ as defined in
 57 Fig.1. Point P is called the pole axis, through which the axis parallel to the z axis is called the pole axis.

58 To derive the analytical model for a thin-walled composite beam, the following assumptions are made:

- 59 1. The contour of the thin wall does not deform in its own plane.
- 60 2. Transverse shear strains $\gamma_{xz}^{\circ}, \gamma_{yz}^{\circ}$ and warping shear γ_{ω}° are incorporated. It is assumed that they are uniform
 61 over the cross-sections.
- 62 3. Each laminate is thin and perfectly bonded.
- 63 4. Local buckling is not considered.

64 According to assumption 1, the midsurface displacement components \bar{u}, \bar{v} at a point A in the contour coordinate
 65 system can be expressed in terms of a displacements U, V of the pole P in the x, y directions, respectively, and the
 66 rotation angle Φ about the pole axis,

$$\bar{u}(s, z) = U(z) \sin \theta(s) - V(z) \cos \theta(s) - \Phi(z)q(s) \quad (1a)$$

$$\bar{v}(s, z) = U(z) \cos \theta(s) + V(z) \sin \theta(s) + \Phi(z)r(s) \quad (1b)$$

67 These equations apply to the whole contour. The out-of-plane shell displacement \bar{w} can now be found from the
 68 assumption 2. For each element of middle surface, the midsurface shear strains in the contour can be expressed with
 69 respect to the transverse shear and warping shear strains.

$$\bar{\gamma}_{nz}(s, z) = \gamma_{xz}^{\circ}(z) \sin \theta(s) - \gamma_{yz}^{\circ}(z) \cos \theta(s) - \gamma_{\omega}^{\circ}(z)q(s) \quad (2a)$$

$$\bar{\gamma}_{sz}(s, z) = \gamma_{xz}^{\circ}(z) \cos \theta(s) + \gamma_{yz}^{\circ}(z) \sin \theta(s) + \gamma_{\omega}^{\circ}(z)r(s) \quad (2b)$$

70 Further, it is assumed that midsurface shear strain in $s - n$ direction is zero ($\bar{\gamma}_{sn} = 0$). From the definition of the

71 shear strain, $\bar{\gamma}_{sz} = 0$ can also be given for each element of middle surface as:

$$\bar{\gamma}_{sz}(s, z) = \frac{\partial \bar{v}}{\partial z} + \frac{\partial \bar{w}}{\partial s} \quad (3)$$

72 After substituting for \bar{v} from Eq.(1) into Eq.(3) and considering the following geometric relations,

$$dx = ds \cos \theta \quad (4a)$$

$$dy = ds \sin \theta \quad (4b)$$

73 Displacement \bar{w} can be integrated with respect to s from the origin to an arbitrary point on the contour,

$$\bar{w}(s, z) = W(z) + \Psi_y(z)x(s) + \Psi_x(z)y(s) + \Psi_\omega(z)\omega(s) \quad (5)$$

74 where Ψ_x, Ψ_y and Ψ_ω represent rotations of the cross section with respect to x, y and ω , respectively, given by:

$$\Psi_y = \gamma_{xz}^\circ(z) - U' \quad (6a)$$

$$\Psi_x = \gamma_{yz}^\circ(z) - V' \quad (6b)$$

$$\Psi_\omega = \gamma_\omega^\circ(z) - \Phi' \quad (6c)$$

75 When the transverse shear effect is ignored, Eq.(6) degenerates to $\Psi_y = -U'$, $\Psi_x = -V'$ and $\Psi_\omega = -\Phi'$. As a result,
76 the number of unknown variables reduces to four leading to the Euler-Bernoulli beam model. The prime (') is used
77 to indicate differentiation with respect to z ; and ω is the so-called sectorial coordinate or warping function given by

$$\omega(s) = \int_{s_0}^s r(s) ds \quad (7a)$$

78 The displacement components u, v, w representing the deformation of any generic point on the profile section are
79 given with respect to the midsurface displacements $\bar{u}, \bar{v}, \bar{w}$ by assuming the first order variation of inplane displacements
80 v, w through the thickness of the contour as:

$$u(s, z, n) = \bar{u}(s, z) \quad (8a)$$

$$v(s, z, n) = \bar{v}(s, z) + n\bar{\psi}_s(s, z) \quad (8b)$$

$$w(s, z, n) = \bar{w}(s, z) + n\bar{\psi}_z(s, z) \quad (8c)$$

81 where, $\bar{\psi}_s$ and $\bar{\psi}_z$ denote the rotations of a transverse normal about the z and s axis, respectively. These functions
82 can be determined by considering that the midsurface shear strains γ_{nz} is given by definition:

$$\bar{\gamma}_{nz}(s, z) = \frac{\partial \bar{w}}{\partial n} + \frac{\partial \bar{u}}{\partial z} \quad (9)$$

83 By comparing Eq.(2) and (9), the function can $\bar{\psi}_z$ can be written as

$$\bar{\psi}_z = \Psi_y \sin \theta - \Psi_x \cos \theta - \Psi_\omega q \quad (10)$$

84 Similarly, using the assumption that the shear strain γ_{sn} should vanish at midsurface, the function $\bar{\psi}_s$ can be obtained

$$\bar{\psi}_s = -\frac{\partial \bar{u}}{\partial s} \quad (11)$$

85 The strains associated with the small-displacement theory of elasticity are given by

$$\epsilon_s(s, z, n) = \bar{\epsilon}_s(s, z) + n\bar{\kappa}_s(s, z) \quad (12a)$$

$$\epsilon_z(s, z, n) = \bar{\epsilon}_z(s, z) + n\bar{\kappa}_z(s, z) \quad (12b)$$

$$\gamma_{sz}(s, z, n) = \bar{\gamma}_{sz}(s, z) + n\bar{\kappa}_{sz}(s, z) \quad (12c)$$

$$\gamma_{nz}(s, z, n) = \bar{\gamma}_{nz}(s, z) + n\bar{\kappa}_{nz}(s, z) \quad (12d)$$

86 where

$$\bar{\epsilon}_s = \frac{\partial \bar{v}}{\partial s}; \quad \bar{\epsilon}_z = \frac{\partial \bar{w}}{\partial z} \quad (13a)$$

$$\bar{\kappa}_s = \frac{\partial \bar{\psi}_s}{\partial s}; \quad \bar{\kappa}_z = \frac{\partial \bar{\psi}_z}{\partial z} \quad (13b)$$

$$\bar{\kappa}_{sz} = \frac{\partial \bar{\psi}_z}{\partial s} + \frac{\partial \bar{\psi}_s}{\partial z}; \quad \bar{\kappa}_{nz} = 0 \quad (13c)$$

87 All the other strains are identically zero. In Eq.(13), $\bar{\epsilon}_s$ and $\bar{\kappa}_s$ are assumed to be zero, and $\bar{\epsilon}_z$, $\bar{\kappa}_z$ and $\bar{\kappa}_{sz}$ are

88 midsurface axial strain and biaxial curvature of the shell, respectively. The above shell strains can be converted to

89 beam strain components by substituting Eqs.(1), (5) and (8) into Eq.(13) as

$$\bar{\epsilon}_z = \epsilon_z^\circ + x\kappa_y + y\kappa_x + \omega\kappa_\omega \quad (14a)$$

$$\bar{\kappa}_z = \kappa_y \sin \theta - \kappa_x \cos \theta - \kappa_\omega q \quad (14b)$$

$$\bar{\kappa}_{sz} = \kappa_{sz} \quad (14c)$$

90 where $\epsilon_z^\circ, \kappa_x, \kappa_y, \kappa_\omega$ and κ_{sz} are axial strain, biaxial curvatures in the x and y direction, warping curvature with

91 respect to the shear center, and twisting curvature in the beam, respectively defined as

$$\epsilon_z^\circ = W' \quad (15a)$$

$$\kappa_x = \Psi'_x \quad (15b)$$

$$\kappa_y = \Psi'_y \quad (15c)$$

$$\kappa_\omega = \Psi'_\omega \quad (15d)$$

$$\kappa_{sz} = \Phi' - \Psi_\omega \quad (15e)$$

92 The resulting strains can be obtained from Eqs.(12) and (14) as

$$\epsilon_z = \epsilon_z^\circ + (x + n \sin \theta) \kappa_y + (y - n \cos \theta) \kappa_x + (\omega - nq) \kappa_\omega \quad (16a)$$

$$\gamma_{sz} = \gamma_{xz}^\circ \cos \theta + \gamma_{yz}^\circ \sin \theta + \gamma_\omega^\circ r + n \kappa_{sz} \quad (16b)$$

$$\gamma_{nz} = \gamma_{xz}^\circ \sin \theta - \gamma_{yz}^\circ \cos \theta - \gamma_\omega^\circ q \quad (16c)$$

93 III. VARIATIONAL FORMULATION

94 The total potential energy of the system can be stated, in its buckled shape, as

$$\Pi = \mathcal{U} + \mathcal{V} \quad (17)$$

95 where \mathcal{U} is the strain energy

$$\mathcal{U} = \frac{1}{2} \int_v (\sigma_z \epsilon_z + \sigma_{sz} \gamma_{sz} + \sigma_{nz} \gamma_{nz}) dv \quad (18)$$

96 After substituting Eq.(16) into Eq.(18)

$$\begin{aligned} \mathcal{U} = & \frac{1}{2} \int_v \left\{ \sigma_z \left[\epsilon_z^\circ + (x + n \sin \theta) \kappa_y + (y - n \cos \theta) \kappa_x + (\omega - nq) \kappa_\omega \right] \right. \\ & \left. + \sigma_{sz} \left[\gamma_{xz}^\circ \cos \theta + \gamma_{yz}^\circ \sin \theta + \gamma_\omega^\circ r + n \kappa_{sz} \right] + \sigma_{nz} \left[\gamma_{xz}^\circ \sin \theta - \gamma_{yz}^\circ \cos \theta + \gamma_\omega^\circ q \right] \right\} dv \end{aligned} \quad (19)$$

97 The variation of strain energy, Eq.(19), can be stated as

$$\delta \mathcal{U} = \int_0^l (N_z \delta \epsilon_z + M_y \delta \kappa_y + M_x \delta \kappa_x + M_\omega \delta \kappa_\omega + V_x \delta \gamma_{xz}^\circ + V_y \delta \gamma_{yz}^\circ + T \delta \gamma_\omega^\circ + M_t \delta \kappa_{sz}) dz \quad (20)$$

98 where $N_z, M_x, M_y, M_\omega, V_x, V_y, T, M_t$ are axial force, bending moments in the x - and y -directions, warping mo-
99 ment (bimoment), and torsional moment with respect to the centroid, respectively, defined by integrating over the

100 cross-sectional area A as

$$N_z = \int_A \sigma_z dsdn \quad (21a)$$

$$M_y = \int_A \sigma_z (x + n \sin \theta) dsdn \quad (21b)$$

$$M_x = \int_A \sigma_z (y - n \cos \theta) dsdn \quad (21c)$$

$$M_\omega = \int_A \sigma_z (\omega - nq) dsdn \quad (21d)$$

$$V_x = \int_A (\sigma_{sz} \cos \theta + \sigma_{nz} \sin \theta) dsdn \quad (21e)$$

$$V_y = \int_A (\sigma_{sz} \sin \theta - \sigma_{nz} \cos \theta) dsdn \quad (21f)$$

$$T = \int_A (\sigma_{sz} r + \sigma_{nz} q) dsdn \quad (21g)$$

$$M_t = \int_A \sigma_{sz} n dsdn \quad (21h)$$

101 The potential of in-plane loads \mathcal{V} due to transverse deflection

$$\mathcal{V} = \frac{1}{2} \int_v \bar{\sigma}_z^0 [(u')^2 + (v')^2] dv \quad (22)$$

102 where $\bar{\sigma}_z^0$ is the averaged constant in-plane edge axial stress, defined by $\bar{\sigma}_z^0 = P^0/A$. The variation of the potential

103 of in-plane loads at the centroid is expressed by substituting the assumed displacement field into Eq.(22) as

$$\begin{aligned} \delta \mathcal{V} = \int_v \frac{P^0}{A} & \left[U' \delta U' + V' \delta V' + (q^2 + r^2 + 2rn + n^2) \Phi' \delta \Phi' + (\Phi' \delta U' + U' \delta \Phi') [n \cos \theta - (y - y_p)] \right. \\ & \left. + (\Phi' \delta V' + V' \delta \Phi') [n \cos \theta + (x - x_p)] \right] dv \end{aligned} \quad (23)$$

104 The kinetic energy of the system is given by

$$\mathcal{T} = \frac{1}{2} \int_v \rho (\dot{u}^2 + \dot{v}^2 + \dot{w}^2) dv \quad (24)$$

105 where ρ is a density.

106 The variation of the kinetic energy is expressed by substituting the assumed displacement field into Eq.(24) as

$$\begin{aligned}
\delta\mathcal{T} = & \int_v \rho \left\{ \delta\dot{W} \left[\dot{W} + \dot{\Psi}_x(y - n \cos \theta) + \dot{\Psi}_y(x + n \sin \theta) + \dot{\Psi}_\omega(\omega - nq) \right] \right. \\
& + \delta\dot{U} \left[\dot{U} + \dot{\Phi} \left[n \cos \theta - (y - y_p) \right] \right] + \delta\dot{V} \left[m_0 \dot{V} + \dot{\Phi} \left[n \sin \theta + (x - x_p) \right] \right] \\
& + \delta\dot{\Phi} \dot{\Phi} \left[\dot{U} \left[n \cos \theta - (y - y_p) \right] + \dot{V} \left[n \sin \theta + (x - x_p) \right] + \dot{\Phi} (q^2 + r^2 + 2rn + n^2) \right] \\
& + \delta\dot{\Psi}_x \dot{\Psi}_x \left[\dot{W} (y - n \cos \theta) + \dot{\Psi}_x (y - n \cos \theta)^2 + \dot{\Psi}_y (x + n \sin \theta) (y - n \cos \theta) + \dot{\Psi}_\omega (y - n \cos \theta) (\omega - nq) \right] \\
& + \delta\dot{\Psi}_y \dot{\Psi}_y \left[\dot{W} (x + n \sin \theta) + \dot{\Psi}_x (x + n \sin \theta) (y - n \cos \theta) + \dot{\Psi}_y (x + n \sin \theta)^2 + \dot{\Psi}_\omega (x + n \sin \theta) (\omega - nq) \right] \\
& \left. + \delta\dot{\Psi}_\omega \dot{\Psi}_\omega \left[\dot{W} (\omega - nq) + \dot{\Psi}_x (y - n \cos \theta) (\omega - nq) + \dot{\Psi}_y (x + n \sin \theta) (\omega - nq) + \dot{\Psi}_\omega (\omega - nq)^2 \right] \right\} dv \quad (25)
\end{aligned}$$

107 In Eqs.(23) and (25), the following geometric relations are used (Fig.1)

$$x - x_p = q \cos \theta + r \sin \theta \quad (26a)$$

$$y - y_p = q \sin \theta - r \cos \theta \quad (26b)$$

108 In order to derive the equations of motion, Hamilton's principle is used

$$\delta \int_{t_1}^{t_2} (\mathcal{T} - \Pi) dt = 0 \quad (27)$$

109 Substituting Eqs.(20), (23) and (25) into Eq.(27), the following weak statement is obtained

$$\begin{aligned}
0 = & \int_{t_1}^{t_2} \int_0^l \left\{ \delta\dot{W} \left[m_0 \dot{W} - m_c \dot{\Psi}_x + m_s \dot{\Psi}_y + (m_\omega - m_q) \dot{\Psi}_\omega \right] + \delta\dot{U} \left[m_0 \dot{U} + (m_c + y_p m_0) \dot{\Phi} \right] \right. \\
& + \delta\dot{V} \left[m_0 \dot{V} + (m_s - x_p m_0) \dot{\Phi} \right] + \delta\dot{\Phi} \left[(m_c + y_p m_0) \dot{U} + (m_s - x_p m_0) \dot{V} + (m_p + m_2 + 2m_r) \dot{\Phi} \right] \\
& + \delta\dot{\Psi}_x \left[-m_c \dot{W} + (m_{y2} - 2m_{yc} + m_{c2}) \dot{\Psi}_x + (m_{xycs} - m_{cs}) \dot{\Psi}_y + (m_{y\omega} - m_{y\omega qc} + m_{qc}) \dot{\Psi}_\omega \right] \\
& + \delta\dot{\Psi}_y \left[m_s \dot{W} + (m_{xycs} - m_{cs}) \dot{\Psi}_x + (m_{x2} + 2m_{xs} + m_{s2}) \dot{\Psi}_y + (m_{x\omega} + m_{x\omega qs} - m_{qs}) \dot{\Psi}_\omega \right] \\
& + \delta\dot{\Psi}_\omega \left[(m_\omega - m_q) \dot{W} + (m_{y\omega} - m_{y\omega qc} + m_{qc}) \dot{\Psi}_x + (m_{x\omega} + m_{x\omega qs} - m_{qs}) \dot{\Psi}_y + (m_{\omega 2} - 2m_{q\omega} + m_{q2}) \dot{\Psi}_\omega \right] \\
& - P^0 \left[\delta U' (U' + \Phi' y_p) + \delta V' (V' - \Phi' x_p) + \delta \Phi' \left(\Phi' \frac{I_p}{A} + U' y_p - V' x_p \right) \right] - N_z \delta W' \\
& \left. - M_y \delta \Psi'_y - M_x \delta \Psi'_x - M_\omega \delta \Psi'_\omega - V_x \delta (U' + \Psi_y) - V_y \delta (V' + \Psi_x) - T \delta (\Phi' - \Psi_\omega) - M_t \delta (\Phi' - \Psi_\omega) \right\} dz dt \quad (28)
\end{aligned}$$

110 All the inertia coefficients in Eq.(28) are given in Ref.[24].

111 **IV. CONSTITUTIVE EQUATIONS**

112 The constitutive equations of a k^{th} orthotropic lamina in the laminate co-ordinate system of section are given by

$$\begin{Bmatrix} \sigma_z \\ \sigma_{sz} \end{Bmatrix}^k = \begin{bmatrix} \bar{Q}_{11}^* & \bar{Q}_{16}^* \\ \bar{Q}_{16}^* & \bar{Q}_{66}^* \end{bmatrix}^k \begin{Bmatrix} \epsilon_z \\ \gamma_{sz} \end{Bmatrix} \quad (29)$$

113 where \bar{Q}_{ij}^* are transformed reduced stiffnesses. The transformed reduced stiffnesses can be calculated from the
 114 transformed stiffnesses based on the plane stress ($\sigma_s = 0$) and plane strain ($\epsilon_s = 0$) assumption. More detailed
 115 explanation can be found in Ref.[26]

116 The constitutive relation for out-of-plane stress and strain is given by

$$\sigma_{nz} = \bar{Q}_{55} \gamma_{nz} \quad (30)$$

117 The constitutive equations for bar forces and bar strains are obtained by using Eqs.(16), (21) and (29)

$$\begin{Bmatrix} N_z \\ M_y \\ M_x \\ M_\omega \\ M_t \\ V_x \\ V_y \\ T \end{Bmatrix} = \begin{bmatrix} E_{11} & E_{12} & E_{13} & E_{14} & E_{15} & E_{16} & E_{17} & E_{18} \\ & E_{22} & E_{23} & E_{24} & E_{25} & E_{26} & E_{27} & E_{28} \\ & & E_{33} & E_{34} & E_{35} & E_{36} & E_{37} & E_{38} \\ & & & E_{44} & E_{45} & E_{46} & E_{47} & E_{48} \\ & & & & E_{55} & E_{56} & E_{57} & E_{58} \\ & & & & & E_{66} & E_{67} & E_{68} \\ & & & & & & E_{77} & E_{78} \\ & & & & & & & E_{88} \end{bmatrix} \begin{Bmatrix} \epsilon_z^\circ \\ \kappa_y \\ \kappa_x \\ \kappa_\omega \\ \kappa_{sz} \\ \gamma_{xz}^\circ \\ \gamma_{yz}^\circ \\ \gamma_\omega^\circ \end{Bmatrix} \quad (31)$$

118 where E_{ij} are stiffnesses of thin-walled composite beams and given in Ref.[23].

119 **V. EQUATIONS OF MOTION**

120 The equations of motion of the present study can be obtained by integrating the derivatives of the varied quantities
 121 by parts and collecting the coefficients of $\delta W, \delta U, \delta V, \delta\Phi, \delta\Psi_y, \delta\Psi_x$ and $\delta\Psi_\omega$

$$N'_z = m_0\ddot{W} - m_c\ddot{\Psi}_x + m_s\ddot{\Psi}_y + (m_\omega - m_q)\ddot{\Psi}_\omega \quad (32a)$$

$$V'_x + P^0(U'' + \Phi''y_p) = m_0\ddot{U} + (m_c + y_pm_0)\ddot{\Phi} \quad (32b)$$

$$V'_y + P^0(V'' - \Phi''x_p) = m_0\ddot{V} + (m_s - x_pm_0)\ddot{\Phi} \quad (32c)$$

$$M'_t + T' + P^0\left(\Phi''\frac{I_p}{A} + U''y_p - V''x_p\right) = (m_c - m_y + y_pm_0)\ddot{U} + (m_s - x_pm_0)\ddot{V} + (m_p + m_2 + 2m_r)\ddot{\Phi} \quad (32d)$$

$$M'_y - V_x = m_s\ddot{W} + (m_{xycs} - m_{cs})\ddot{\Psi}_x + (m_{x2} + 2m_{xs} + m_{s2})\ddot{\Psi}_y \quad (32e)$$

$$+ (m_{x\omega} + m_{x\omega qs} - m_{qs})\ddot{\Psi}_\omega \quad (32f)$$

$$M'_x - V_y = -m_c\ddot{W} + (m_{y2} - 2m_{yc} + m_{c2})\ddot{\Psi}_x + (m_{xycs} - m_{cs})\ddot{\Psi}_y \quad (32g)$$

$$+ (m_{y\omega} - m_{y\omega qc} + m_{qc})\ddot{\Psi}_\omega \quad (32h)$$

$$M'_\omega + M_t - T = (m_\omega - m_q)\ddot{W} + (m_{y\omega} - m_{y\omega qc} + m_{qc})\ddot{\Psi}_x \quad (32i)$$

$$+ (m_{x\omega} + m_{x\omega qs} - m_{qs})\ddot{\Psi}_y$$

$$+ (m_{\omega 2} - 2m_{q\omega} + m_{q2})\ddot{\Psi}_\omega \quad (32j)$$

122 The natural boundary conditions are of the form

$$\delta W : \quad W = \bar{W}_0 \quad \text{or} \quad N_z = \bar{N}_{z_0} \quad (33a)$$

$$\delta U : \quad U = \bar{U}_0 \quad \text{or} \quad V_x = \bar{V}_{x_0} \quad (33b)$$

$$\delta V : \quad V = \bar{V}_0 \quad \text{or} \quad V_y = \bar{V}_{y_0} \quad (33c)$$

$$\delta\Phi : \quad \Phi = \bar{\Phi}_0 \quad \text{or} \quad T + M_t = \bar{T}_0 + \bar{M}_{t_0} \quad (33d)$$

$$\delta\Psi_y : \quad \Psi_y = \bar{\Psi}_{y_0} \quad \text{or} \quad M_y = \bar{M}_{y_0} \quad (33e)$$

$$\delta\Psi_x : \quad \Psi_x = \bar{\Psi}_{x_0} \quad \text{or} \quad M_x = \bar{M}_{x_0} \quad (33f)$$

$$\delta\Psi_\omega : \quad \Psi_\omega = \bar{\Psi}_{\omega_0} \quad \text{or} \quad M_\omega = \bar{M}_{\omega_0} \quad (33g)$$

123 The 7th denotes the warping restraint boundary condition. When the warping of the cross section is restrained,
 124 $\Psi_\omega = 0$ and when the warping is not restrained, $M_\omega = 0$.

Eq.(32) is most general form for axial-flexural-torsional-shearing vibration and buckling of thin-walled composite beams. For general anisotropic materials, the dependent variables, U , V , W , Φ , Ψ_x , Ψ_y and Ψ_ω are fully-coupled implying that the beam undergoes a coupled behavior involving bending, extension, twisting, transverse shearing, and warping. The resulting coupling is referred to as sixfold coupled vibration and buckling. If all the coupling effects and the inertia coefficients are neglected as well as cross section is symmetrical with respect to both x - and the y -axes, Eq.(32) can be simplified to the uncoupled differential equations as

$$(EA)_{com} W'' = 0 \quad (34a)$$

$$(GA_y)_{com}(U'' + \Psi'_y) + P^0 U'' = 0 \quad (34b)$$

$$(GA_x)_{com}(V'' + \Psi'_x) + P^0 V'' = 0 \quad (34c)$$

$$\left[(GJ_1)_{com} + P^0 \frac{I_p}{A} \right] \Phi'' - (GJ_2)_{com} \Psi'_\omega = 0 \quad (34d)$$

$$(EI_y)_{com} \Psi''_y - (GA_y)_{com}(U' + \Psi_y) = 0 \quad (34e)$$

$$(EI_x)_{com} \Psi''_x - (GA_x)_{com}(V' + \Psi_x) = 0 \quad (34f)$$

$$(EI_\omega)_{com} \Psi''_\omega + (GJ_2)_{com} \Phi' - (GJ_1)_{com} \Psi_\omega = 0 \quad (34g)$$

From above equations, $(EA)_{com}$ represents axial rigidity, $(GA_x)_{com}$, $(GA_y)_{com}$ represent shear rigidities with respect to x and y axis, $(EI_x)_{com}$ and $(EI_y)_{com}$ represent flexural rigidities with respect to x - and y -axis, $(EI_\omega)_{com}$ represents warping rigidity, and $(GJ_1)_{com}$, $(GJ_2)_{com}$, $(GJ)_{com}$ represent torsional rigidities of thin-walled composite beams, respectively, written as

$$(EA)_{com} = E_{11} \quad (35a)$$

$$(EI_y)_{com} = E_{22} \quad (35b)$$

$$(EI_x)_{com} = E_{33} \quad (35c)$$

$$(EI_\omega)_{com} = E_{44} \quad (35d)$$

$$(GA_y)_{com} = E_{66} \quad (35e)$$

$$(GA_x)_{com} = E_{77} \quad (35f)$$

$$(GA_\omega)_{com} = E_{88} \quad (35g)$$

$$(GJ_1)_{com} = E_{55} + E_{88} \quad (35h)$$

$$(GJ_2)_{com} = E_{55} - E_{88} \quad (35i)$$

$$(GJ)_{com} = 4E_{55} \quad (35j)$$

135 It is well known that the three distinct buckling modes, flexural buckling in the x - and y -direction, and torsional
 136 buckling, are identified in this case, and the corresponding buckling loads are given by orthotropy solution for a
 137 clamped beam boundary conditions [10]

$$P_x = \left[\frac{(0.5l)^2}{\pi^2(EI_x)_{com}} + \frac{1}{(GA_x)_{com}} \right]^{-1} \quad (36a)$$

$$P_y = \left[\frac{(0.5l)^2}{\pi^2(EI_y)_{com}} + \frac{1}{(GA_y)_{com}} \right]^{-1} \quad (36b)$$

$$P_\theta = \frac{A}{I_p} \left[\left[\frac{(0.5l)^2}{\pi^2(EI_\omega)_{com}} + \frac{1}{(GA_\omega)_{com}} \right]^{-1} + (GJ)_{com} \right] \quad (36c)$$

138 where P_x, P_y, P_θ are flexural buckling loads in the x - and y -direction, and torsional buckling load, respectively.

139 VI. FINITE ELEMENT FORMULATION

140 The present theory for thin-walled composite beams described in the previous section was implemented via a
 141 one-dimensional displacement-based finite element method. The generalized displacements are expressed over each
 142 element as a linear combination of the one-dimensional Lagrange interpolation function $\widehat{\phi}_j$ associated with node j
 143 and the nodal values

$$W = \sum_{j=1}^n w_j \widehat{\phi}_j \quad (37a)$$

$$U = \sum_{j=1}^n u_j \widehat{\phi}_j \quad (37b)$$

$$V = \sum_{j=1}^n v_j \widehat{\phi}_j \quad (37c)$$

$$\Phi = \sum_{j=1}^n \phi_j \widehat{\phi}_j \quad (37d)$$

$$\Psi_y = \sum_{j=1}^n \psi_{yj} \widehat{\phi}_j \quad (37e)$$

$$\Psi_x = \sum_{j=1}^n \psi_{xj} \widehat{\phi}_j \quad (37f)$$

$$\Psi_\omega = \sum_{j=1}^n \psi_{\omega j} \widehat{\phi}_j \quad (37g)$$

144

145 Substituting these expressions into the weak statement in Eq.(28), the finite element model of a typical element
 146 can be expressed as

$$([K] - P^0[G] - \omega^2[M])\{\Delta\} = \{0\} \quad (38)$$

147 where $[K], [M]$ are the element stiffness matrix, the element mass matrix and given in Ref.[24]. The element
148 geometric stiffness matrix $[G]$ are defined by

$$[G] = \begin{bmatrix} G_{11} & G_{12} & G_{13} & G_{14} & G_{15} & G_{16} & G_{17} \\ & G_{22} & G_{23} & G_{24} & G_{25} & G_{26} & G_{27} \\ & & G_{33} & G_{34} & G_{35} & G_{36} & G_{37} \\ & & & G_{44} & G_{45} & G_{46} & G_{47} \\ & & & & G_{55} & G_{56} & G_{57} \\ & & & & & G_{66} & G_{67} \\ \text{sym.} & & & & & & G_{77} \end{bmatrix} \quad (39)$$

149 The explicit forms of $[G]$ are given by

$$G_{ij}^{22} = G_{ij}^{33} = \int_0^l \psi'_i \psi'_j dz \quad (40a)$$

$$G_{ij}^{24} = \int_0^l y_p \psi'_i \psi'_j dz \quad (40b)$$

$$G_{ij}^{34} = - \int_0^l x_p \psi'_i \psi'_j dz \quad (40c)$$

$$G_{ij}^{44} = \int_0^l \frac{I_p}{A} \psi'_i \psi'_j dz \quad (40d)$$

150 All other components are zero.

151 In Eq.(38), $\{\Delta\}$ is the eigenvector of nodal displacements corresponding to an eigenvalue

$$\{\Delta\} = \{W \ U \ V \ \Phi \ \Psi_y \ \Psi_x \ \Psi_\omega\}^T \quad (41)$$

152 VII. NUMERICAL EXAMPLES

153 For verification purpose, the buckling behavior and free vibration of a cantilever isotropic mono-symmetric channel
154 section beam, as shown in Fig.2, with length $l = 2\text{m}$ under axial force at the centroid is performed. Throughout
155 the numerical examples, ten quadratic elements with three nodes are used. The material properties are assumed to
156 be: $E = 0.3\text{GPa}$, $G = 0.115\text{GPa}$, $\rho = 7850\text{kg/m}^3$. The buckling loads and natural frequencies are evaluated and

157 compared with numerical results of Kim et al.[27] which is based on dynamic stiffness formulation and ABAQUS
 158 solutions in Table I. The present results are in a good agreement with those by Kim et al.[27].

159 In the next example, a simply-supported composite I-beam with a span of 6.0m under axial force applied to the
 160 centroid is analyzed. A doubly symmetric I-section of 600mm wide flange and 600mm deep web is considered. The
 161 flanges and web are made of four plies with each ply 7.5mm in thickness. The material is graphite-epoxy whose layer
 162 properties are defined: $E_1 = 144\text{GPa}$, $E_2 = 9.65\text{GPa}$, $G_{12} = G_{13} = 4.14\text{GPa}$, $G_{23} = 3.45\text{GPa}$, $\nu_{12} = 0.3$. Plane
 163 stress assumption ($\sigma_s = 0$) is made in the analysis. The critical buckling loads obtained from the present analysis are
 164 given in Table II, along with the finite element results of Machado and Cortinez [16] and Back and Will [19]. It is
 165 observed that the present results are in good agreement with the solutions in Refs.[16,19] for all cases of lay-ups.

166 To demonstrate the accuracy and validity of this study further, a cantilever symmetrically laminated mono-
 167 symmetric I-beam with length $l = 1\text{m}$ under axial load at the centroid is considered. Following dimensions for
 168 the beam are used: the height, top and bottom flange widths are 50mm, 30mm and 50mm, respectively. The flanges
 169 and web are made of sixteen layers with each layer 0.13mm in thickness. All computations are carried out for
 170 the glass-epoxy materials with the following material properties: $E_1 = 53.78\text{GPa}$, $E_2 = 17.93\text{GPa}$, $G_{12} = G_{13} =$
 171 8.96GPa , $G_{23} = 3.45\text{GPa}$, $\nu_{12} = 0.25$. The comparison of the critical buckling loads among the proposed finite
 172 element solution, the analytical approach by Kim et al. [21] are given in Table III for different stacking sequences.
 173 The present finite element solution again indicates good agreement with the analytical solution and ABAQUS results
 174 for all lamination schemes considered.

175 In order to investigate the effects of fiber orientation and shear deformation on the critical buckling loads and the
 176 mode shapes as well as load-frequency interaction curves, thin-walled composite I-beams with different span-to-height
 177 ratios under axial load at the centroid are considered. The geometry and stacking sequences of I-section are shown in
 178 Fig.3, and the following engineering constants are used

$$E_1/E_2 = 25, G_{12}/E_2 = 0.6, G_{13} = G_{12} = G_{23}, \nu_{12} = 0.25 \quad (42)$$

179 For convenience, the following nondimensional buckling load and natural frequency are used

$$\bar{P} = \frac{Pl^2}{b_3^3 t E_2} \quad (43)$$

$$\bar{\omega} = \frac{\omega l^2}{b_3} \sqrt{\frac{\rho}{E_2}} \quad (44)$$

180 The flanges and web are considered as antisymmetric angle-ply laminates $[\theta/-\theta]$, (Fig.3a). For this lay-up, all the
 181 coupling stiffnesses are zero, but E_{35} and E_{38} do not vanish due to unsymmetric stacking sequence of the flanges

182 and web. As the first example, the stacking sequence at two specific fiber angle $\theta = 0^\circ$ and 30° is considered to
 183 investigate the effects of axial force and shear deformation on the fundamental natural frequency. Fig.4 shows the
 184 interaction diagram between flexural-torsional buckling and natural frequency with span-to-height ratio $l/b_3 = 10$.
 185 By using a linear combination of the one-dimensional Lagrange and Hermite-cubic interpolation function in finite
 186 element formulation [22], the load-frequency interaction curves obtained from previous research [25] based on the
 187 classical beam theory are also displayed. It can be seen that the change in the natural frequency due to axial force is
 188 noticeable. The natural frequency diminishes when the axial force changes from tensile to compressive, as expected.
 189 It is obvious that the natural frequency decreases with the increase of axial force, and the decrease becomes more
 190 quickly when the axial force is close to critical buckling load. Moreover, this decrease is more pronounced with fiber
 191 angle $\theta = 0^\circ$ when the shear effects are included in the analysis. With $\theta = 0^\circ$ and 30° , at about $\bar{P}=36.165$ and
 192 12.806, the natural frequencies become zero which implies that at these loads, flexural-torsional bucklings occur as a
 193 degenerate case of natural vibration at zero frequency. It is from Fig.4 that explains the duality between the critical
 194 flexural-torsional buckling load and the fundamental natural frequency.

195 The next example is the same as before except that in this case, the fiber angle is rotated in the flanges and web
 196 (Fig.3a). The critical buckling loads by the finite element analysis (FEM) and the orthotropy solutions, which neglects
 197 the coupling effects of E_{35} , E_{38} , from Eqs.(36a)-(36c) are given in Fig.5. The results with no shear effects calculated
 198 from previous paper [22]. As expected, for classical beam model, the critical buckling loads decrease monotonically
 199 with the increase of fiber angle. However, for present model, after P_{cr} reaches maximum value around $\theta = 10^\circ$, it
 200 decreases. This local maximum occurs because at low fiber angle, large shear effects reduce flexural stiffnesses. It
 201 is interesting to note that the shear effects are negligibly small even for the lower span-to-height ratio ($l/b_3 = 10$),
 202 especially in the interval $\theta \in [30^\circ, 90^\circ]$. This trend can be explained that the flexural stiffnesses decrease significantly
 203 with the increasing fiber angle, and thus, the relative shear effects become smaller for higher fiber angles. Due to
 204 coupling stiffnesses, the orthotropy solution might not be accurate. However, as fiber angle increases, the coupling
 205 effects coming from the material anisotropy become negligible. Therefore, it can be seen in Fig.5, for all fiber angles,
 206 the critical buckling loads by the finite element analysis exactly correspond to the flexural buckling loads in y -direction.
 207 It can be explained partly by the typical mode shapes with the fiber angle $\theta = 30^\circ$ in Fig.6. It is indicated that the
 208 simple orthotropy solution is sufficiently accurate for this lay-up.

209 To investigate the coupling and shear effects further, the same configuration with the previous example except the
 210 lay-up is considered. The bottom flange is considered as $[\theta_2]$, while the top flange and web are $[0/45]$, respectively

211 (Fig.3b). For this lay-up, the coupling stiffnesses $E_{16}, E_{17}, E_{18}, E_{36}, E_{37}$ and E_{68} become no more negligibly small.
 212 Fig.7 displays the effects of shear deformation on the critical buckling loads with two different ratios. For $l/b_3 = 25$,
 213 since the shear effects are negligible, the solutions of two models nearly coincide. However, for lower span-to-height
 214 ratio ($l/b_3 = 5$), it is noticed that discarding shear effects again leads to an overprediction of the critical buckling loads
 215 for all fiber angles especially in the range of $\theta \in [0^\circ, 30^\circ]$. The results by orthotropy solution and the finite element
 216 analysis with $l/b_3 = 5$ are shown in Fig.8. The buckling mode shapes with various fiber angles $\theta = 0^\circ, 15^\circ$ and 75° are
 217 illustrated in Figs.9-11. Three types of mode shapes can be seen. Relative measures of axial, flexural displacements,
 218 torsional and shearing rotations show that, at $\theta = 0^\circ$ when the beam is buckling exhibits fourfold coupled mode
 219 (the flexural mode in y -direction, torsional mode and corresponding shearing mode), whereas, at $\theta = 15^\circ$, the beam
 220 displays three further mode (axial mode, the flexural mode in x -direction and corresponding shearing mode). Due
 221 to small out-of-plane displacement W (Fig.10), the resulting mode shape is referred to as sixfold coupled mode. It
 222 is from this sixfold coupled mode that highlights the influence of coupling and shear effects on the buckling behavior
 223 of thin-walled composite beams. This response is never observed in the classical beam model [22] because the shear
 224 effects are not present. As fiber angle increases, since the coupling stiffnesses decrease, the buckling mode shape
 225 becomes predominantly torsional mode as shown in Fig.11. Consequently, the critical buckling loads by the finite
 226 element analysis exactly correspond to the torsional buckling loads of orthotropy solution. This fact explains as the
 227 fiber angle changes, for lower span-to-height ratio, the orthotropy solutions disagree with the finite element solutions as
 228 anisotropy of the beam gets higher. That is, the orthotropy solution is no longer valid for unsymmetrically laminated
 229 beams, and sixfold coupled flexural-torsional-shearing buckling should be considered even for a doubly symmetric
 230 cross-section.

231 Finally, the effects of span-to-height ratio (l/b_3) and modulus ratio (E_1/E_2) on the critical buckling loads of a
 232 simply supported beam are investigated. The stacking sequence of the flanges and web are $[0/90]_s$, (Fig.3c). For
 233 this lay-up, all the coupling stiffnesses vanish and thus, the critical buckling loads exactly correspond to the flexural
 234 buckling loads in y -direction. It is evident from Fig.12 that the shear-deformable beam theory is very effective in
 235 a relatively large region up to the point where span-to-height ratio reaches value of $l/b_3 = 20$. For this reason, a
 236 span-to-height ratio $l/b_3 = 5$ is chosen to show effect of modulus ratio on the the critical buckling loads. The critical
 237 buckling loads increase as modulus ratio increase in Fig.13. It is obvious that the omission of shear effects causes an
 238 overestimation of the critical buckling loads with increasing orthotropy (E_1/E_2).

239 VIII. CONCLUDING REMARKS

240 A analytical model based on shear-deformable beam theory is presented to study the flexural-torsional buckling of
 241 thin-walled composite beams under axial load. This model is capable of predicting accurately the critical buckling
 242 loads and corresponding mode shapes for various configuration. All of the possible buckling mode shapes including
 243 the flexural mode in the x - and y -direction, the torsional mode, and fully coupled flexural-torsional-shearing mode are
 244 included in the analysis. The shear effects become significant for lower span-to-height ratio. The orthotropy solution
 245 is accurate for lower degrees of material anisotropy, but, becomes inappropriate as the anisotropy of the beam gets
 246 higher, and fully coupled equations should be considered for accurate analysis of thin-walled composite beams. The
 247 present model is found to be appropriate and efficient in analyzing buckling problem of thin-walled composite beams
 248 under axial load.

249 Acknowledgments

250 The support of the research reported here by Seoul R&BD Program through Grant GR070033 is gratefully ac-
 251 knowledged. The authors also would like to thank the anonymous reviewers for their suggestions in improving the
 252 standard of the manuscript.

253 References

- 254 [1] Vlasov VZ. Thin-walled elastic beams. 2nd Edition. Jerusalem, Israel: Israel Program for Scientific Translation, 1961.
- 255 [2] Gjelsvik A. The theory of thin-walled bars. New York: John Wiley and Sons Inc., 1981.
- 256 [3] Timoshenko SV, Gere JM. Theory of Elastic Stability. New York: McGraw-Hill, 1961.
- 257 [4] Trahair NS. Flexural-torsional buckling of structures. London: CRC Press, 1993.
- 258 [5] Pandey MD, Kabir MZ and Sherbourne AN. Flexural-torsional stability of thin-walled composite I-section beams. Compos
 259 Eng 1995; 5(3):321-342.
- 260 [6] Lin ZM, Polyzois D and Shah A. Stability of thin-walled pultruded structural members by the finite element method.
 261 Thin-Walled Struct 1996; 24(1):1-18.
- 262 [7] Shield CK and Morey TA. Kinematic theory of open and closed section thin-walled composite beams. J Eng Mech 1997;
 263 123(10):1070-1081.
- 264 [8] Kollar LP. Flexural-torsional buckling of open section composite columns with shear deformation. Int J Solids Struct 2001;
 265 38(42-43):7525-7541.

- 266 [9] Kollar LP. Flexural-torsional vibration of open section composite columns with shear deformation. *Int J Solids Struct* 2001;
267 38(42-43):7543-7558.
- 268 [10] Kollar LP and Springer GS. *Mechanics of composite structure*. Cambridge University Press, 2003.
- 269 [11] Davalos JF, Qiao P and Salim HA. Flexural-torsional buckling of pultruded fiber reinforced plastic composite I-beams:
270 experimental and analytical evaluations. *Compos Struct* 1997; 38(1-4):241-250.
- 271 [12] Qiao P, Zou G and Davalos JF. Flexural-torsional buckling of fiber-reinforced plastic composite cantilever I-beams. *Compos*
272 *Struct* 2003; 60(2):205-217.
- 273 [13] Shan L and Qiao P. Flexural-torsional buckling of fiber-reinforced plastic composite open channel beams. *Compos Struct*
274 2005; 68(2):211-224.
- 275 [14] Librescu L and Song O. *Thin-walled Composite Beams*. Springer, 2006.
- 276 [15] Cortinez VH and Piovan MT. Vibration and buckling of composite thin-walled beams with shear deformability. *J Sound*
277 *Vib* 2002; 258(4-5):701-723.
- 278 [16] Machado SP and Cortinez VH. Non-linear model for stability of thin-walled composite beams with shear deformation.
279 *Thin-Walled Struct* 2005; 43(10):1615-1645.
- 280 [17] Cortinez VH and Piovan MT. Stability of composite thin-walled beams with shear deformability. *Comput Struct* 2006;
281 84(15-16):978-990.
- 282 [18] Piovan MT and Cortinez VH. Mechanics of shear deformable thin-walled beams made of composite materials. *Thin-Walled*
283 *Struct* 2007; 45(1):37-62
- 284 [19] Back SY and Will KM. Shear-flexible thin-walled element for composite I-beams. *Eng Struct* 2007; 30(5): 1447-1458
- 285 [20] Kim NI, Shin DK and Kim MY. Improved flexural-torsional stability analysis of thin-walled composite beam and exact
286 stiffness matrix. *Int J Mech Sci* 2007; 49(8):950-969.
- 287 [21] Kim NI, Shin DK and Kim MY. Flexural-torsional buckling loads for spatially coupled stability analysis of thin-walled
288 composite columns. *Adv Eng Softw* 2008; 39(12):949-961.
- 289 [22] Lee J and Kim S. Flexural-torsional buckling of thin-walled I-section composites. *Comput Struct* 2001; 79(10):987-995.
- 290 [23] Lee J. Flexural analysis of thin-walled composite beams using shear-deformable beam theory. *Compos Struct* 2005;
291 70(2):212-222.
- 292 [24] Vo TP and Lee J. On sixfold coupled vibrations of thin-walled composite box beams. *Compos Struct* 2008; In Press.
- 293 [25] Vo TP and Lee J. Flexural-torsional coupled vibration of axially loaded thin-walled open-section composite beams. *Thin-*
294 *walled Struct* 2008, submitted.
- 295 [26] Jones RM. *Mechanics of composite materials*. New York: Hemisphere Publishing Corp., 1975.
- 296 [27] Kim MY, Kim NI and Yun HT. Exact dynamic and static stiffness matrices of shear deformable thin-walled beam-columns.
297 *J Sound Vib* 2003; 267(1):29-55.

298 **CAPTIONS OF TABLES**

299 Table I: The bucking loads and natural frequencies a cantilever isotropic mono-symmetric channel section beam.

300 Table II: Critical bucking loads of a simply supported doubly symmetric composite I-beam (10^6N).

301 Table III: Critical bucking loads of a cantilever mono-symmetric composite I-beam (N).

302 **CAPTIONS OF FIGURES**

303 Figure 1: Definition of coordinates and generalized displacements in thin-walled open sections.

304 Figure 2: Isotropic mono-symmetric channel section for verification.

305 Figure 3: Geometry and stacking sequences of thin-walled composite I-beam.

306 Figure 4: The effect of axial force on the fundamental natural frequency with the fiber angle 0° and 30° in the
307 flanges and web of a clamped composite beam with $l/b_3 = 10$.

308 Figure 5: Variation of the critical buckling loads with respect to fiber angle change in the flanges and web of a
309 clamped composite beam with $l/b_3 = 10$.

310 Figure 6: Mode shapes of the flexural-shearing components for $P_{cr} = 12.806$ with the fiber angle 30° in the flanges
311 and web of a clamped composite beam with $l/b_3 = 10$.

312 Figure 7: Variation of the critical buckling loads with respect to fiber angle change in the bottom flange of clamped
313 composite beams with $l/b_3 = 5$ and $l/b_3 = 25$.

314 Figure 8: Variation of the critical buckling loads with respect to fiber angle change in the bottom flange of a
315 clamped composite beam with $l/b_3 = 5$.

316 Figure 9: Mode shapes of the flexural-torsional-shearing components for $P_{cr} = 16.563$ with the fiber angle 0° in the
317 bottom flange of a clamped composite beam with $l/b_3 = 5$.

318 Figure 10: Mode shapes of the flexural-torsional-shearing components for $P_{cr} = 19.059$ with the fiber angle 15° in
319 the bottom flange of a clamped composite beam with $l/b_3 = 5$.

320 Figure 11: Mode shapes of the torsional-shearing components for $P_{cr} = 2.234$ with the fiber angle 75° in the bottom
321 flange of a clamped composite beam with $l/b_3 = 5$.

322 Figure 12: Variation of the critical buckling loads of a simply supported composite beam with respect to span-to-
323 height ratio change.

324 Figure 13: Variation of the critical buckling loads with respect to modulus ratio change of a simply supported
325 composite beam with $l/b_3 = 5$.

TABLE I The buckling loads and natural frequencies a cantilever isotropic mono-symmetric channel section beam.

Mode	Buckling loads (N)			Natural frequencies (rad/s) ²		
	Ref.[27]		Present	Ref.[27]		Present
	ABAQUS	With shear		ABAQUS	With shear	
1	0.027	0.028	0.026	13.789	14.001	12.977
2	0.334	0.331	0.334	111.840	113.100	113.440
3	0.704	0.696	0.707	191.160	190.080	190.567
4	1.065	1.074	1.084	255.100	256.670	263.999

TABLE II Critical bucking loads of a simply supported doubly symmetric composite I-beam (10^6N).

Lay-ups	Ref.[16]		Ref.[19]		Present
	No shear	With shear	ABAQUS	With shear	
$[0]_4$	42.11	33.18	30.78	28.85	30.38
$[30/-30]_s$			13.06	13.17	13.17
$[45/-45]_s$	4.45	4.44	4.40	4.41	4.41
$[60/-60]_s$			2.89	2.89	2.88
$[0/90]_s$	22.57	19.84	20.41	20.63	20.63

TABLE III Critical bucking loads of a cantilever mono-symmetric composite I-beam (N).

Lay-ups	Ref.[21]		Present
	ABAQUS	No shear	
$[0]_{16}$	2969.7	2998.2	2993.2
$[15/-15]_{4s}$	2790.9	2811.8	2803.6
$[30/-30]_{4s}$	2190.6	2199.7	2184.7
$[45/-45]_{4s}$	1558.9	1561.9	1546.0
$[60/-60]_{4s}$	1239.4	1241.3	1227.8
$[75/-75]_{4s}$	1132.2	1134.5	1126.7
$[0/90]_{4s}$	2101.5	2113.9	2100.6

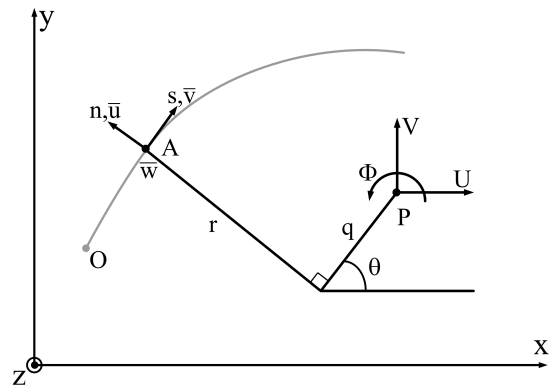


FIG. 1 Definition of coordinates and generalized displacements in thin-walled open sections.

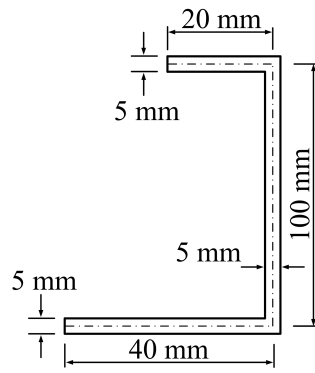


FIG. 2 Isotropic mono-symmetric channel section for verification.

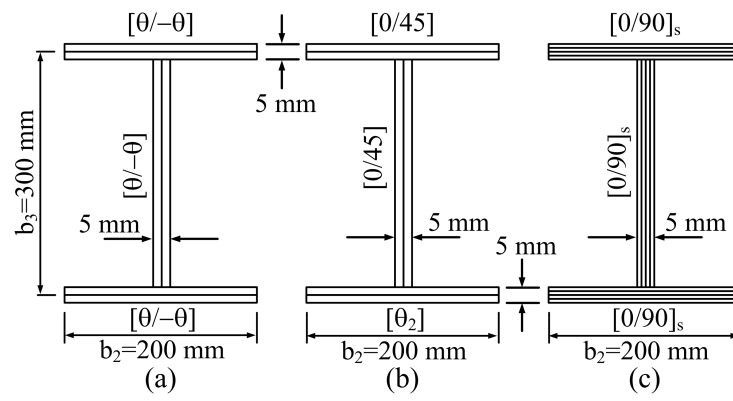


FIG. 3 Geometry and stacking sequences of thin-walled composite I-beam.

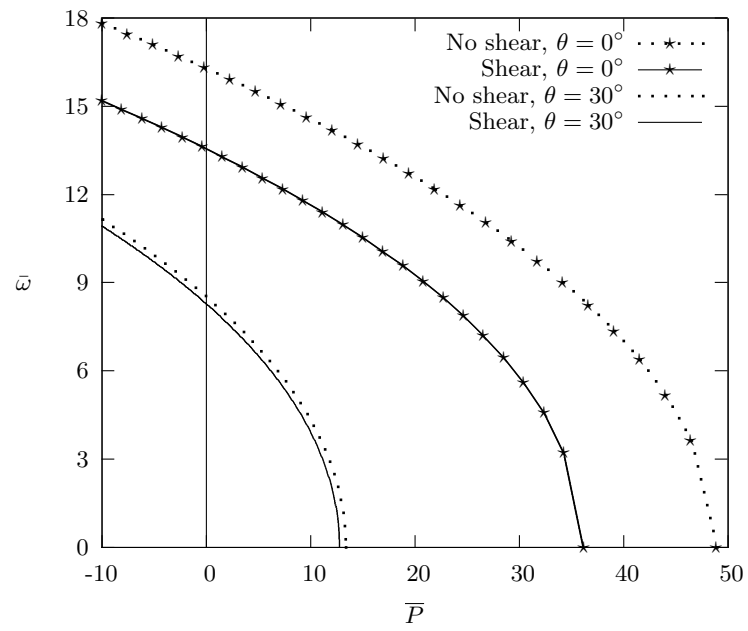


FIG. 4 The effect of axial force on the fundamental natural frequency with the fiber angle 0° and 30° in the flanges and web of a clamped composite beam with $l/b_3 = 10$.

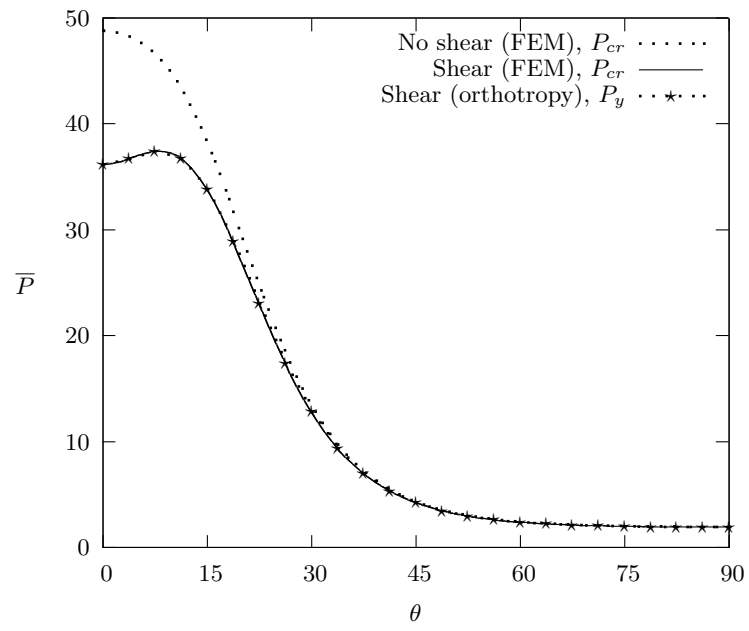


FIG. 5 Variation of the critical buckling loads with respect to fiber angle change in the flanges and web of a clamped composite beam with $l/b_3 = 10$.

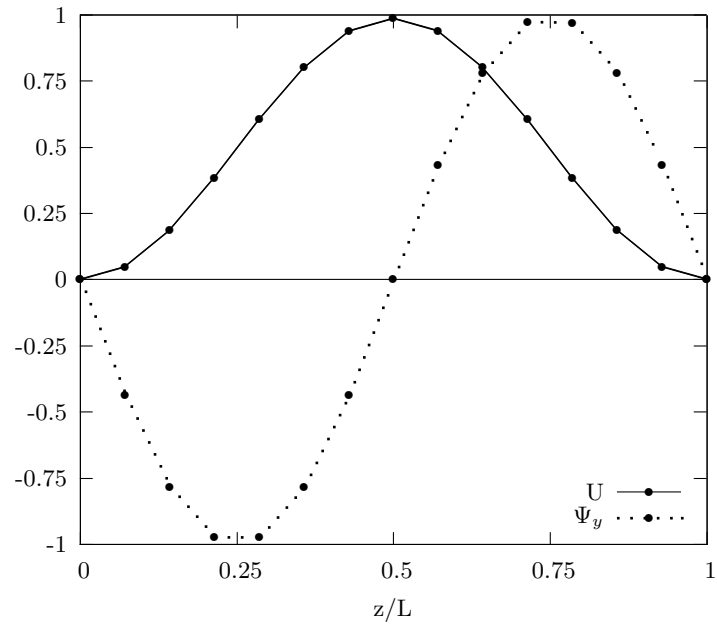


FIG. 6 Mode shapes of the flexural-torsional-shearing components for $P_{cr} = 12.806$ with the fiber angle 30° in the flanges and web of a clamped composite beam with $l/b_3 = 10$.

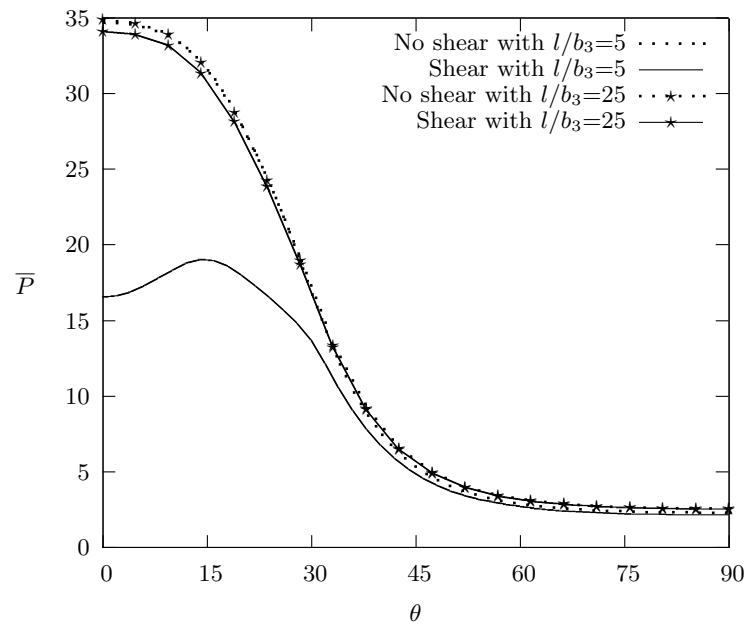


FIG. 7 Variation of the critical buckling loads with respect to fiber angle change in the bottom flange of clamped composite beams with $l/b_3 = 5$ and $l/b_3 = 25$.

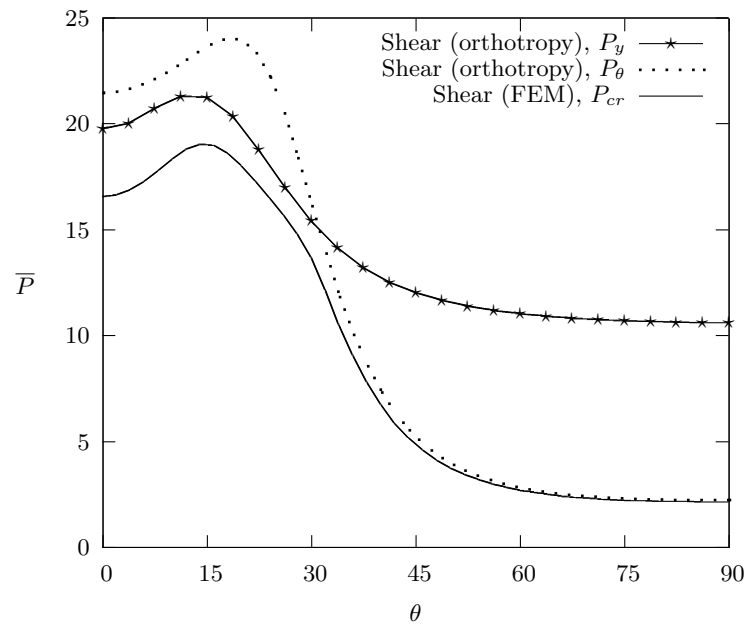


FIG. 8 Variation of the critical buckling loads with respect to fiber angle change in the bottom flange of a clamped composite beam with $l/b_3 = 5$.

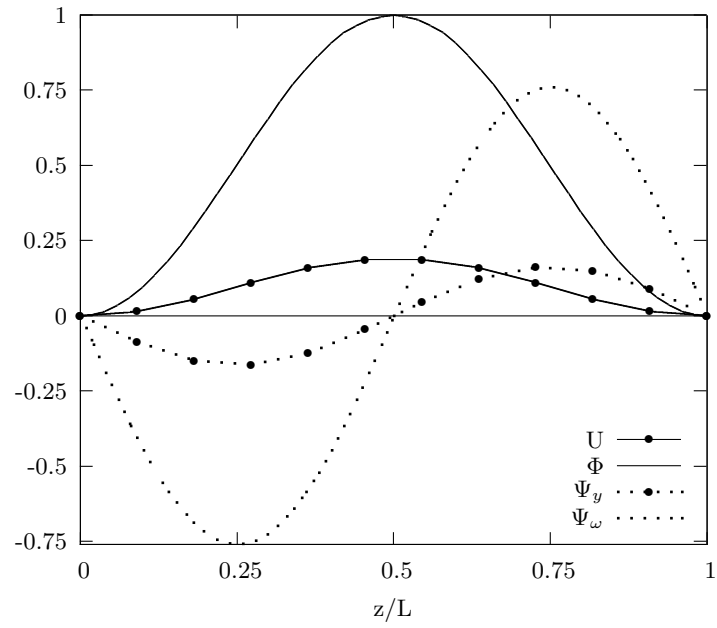


FIG. 9 Mode shapes of the flexural-torsional-shearing components for $P_{cr} = 15.563$ with the fiber angle 0° in the bottom flange of a clamped composite beam with $l/b_3 = 5$.

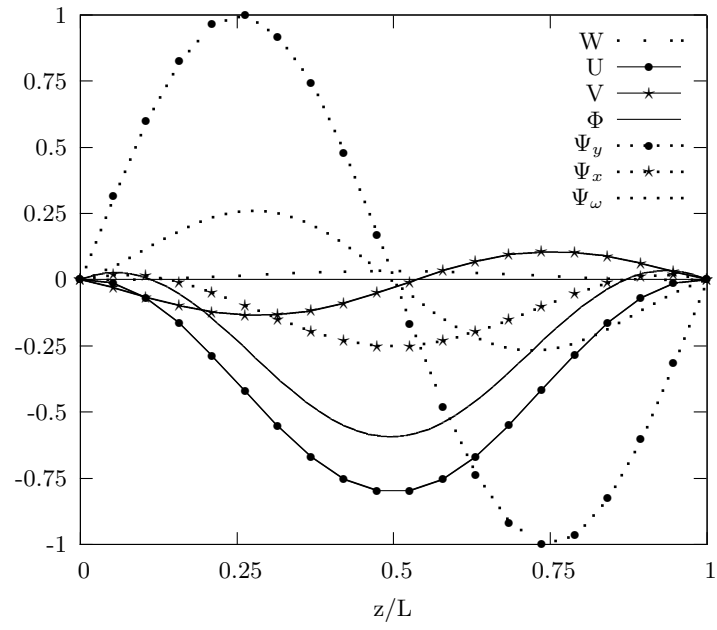


FIG. 10 Mode shapes of the flexural-torsional-shearing components for $P_{cr} = 19.059$ with the fiber angle 15° in the bottom flange of a clamped composite beam with $l/b_3 = 5$.

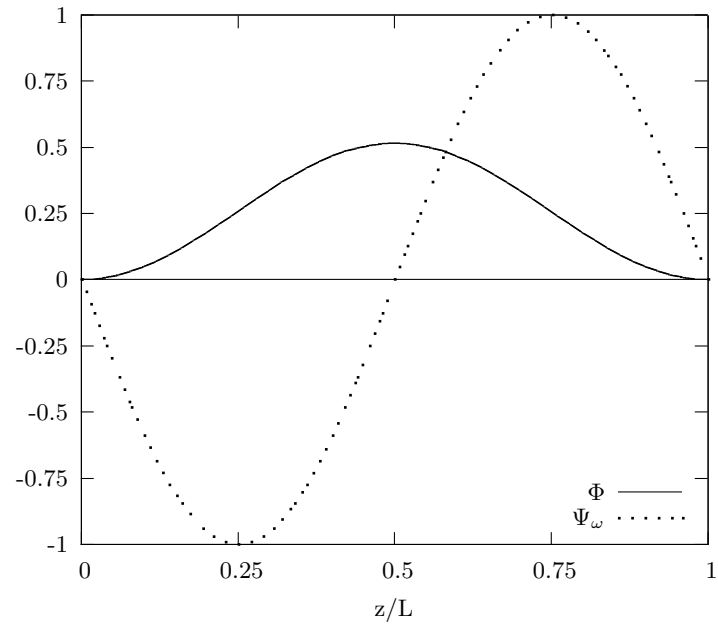


FIG. 11 Mode shapes of the torsional-shearing components for $P_{cr} = 2.234$ with the fiber angle 75° in the bottom flange of a clamped composite beam with $l/b_3 = 5$.

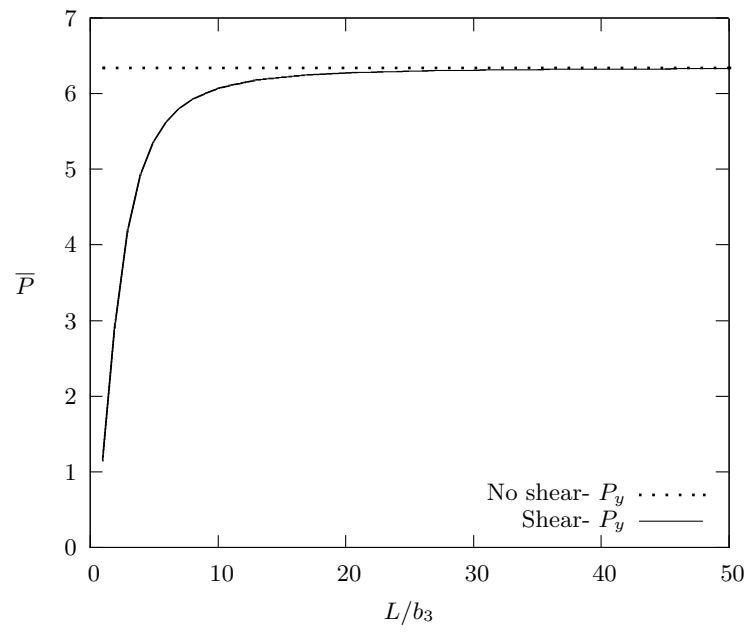


FIG. 12 Variation of the critical buckling loads of a simply supported composite beam with respect to span-to-height ratio change.

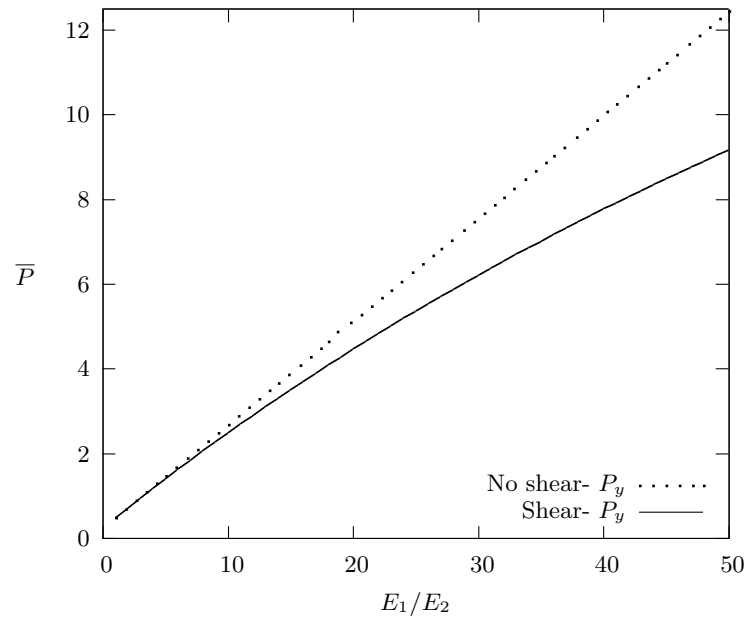


FIG. 13 Variation of the critical buckling loads with respect to modulus ratio change of a simply supported composite beam with $l/b_3 = 5$.